Proceedings of the XXIII Conference on Applied Crystallography, Krynica Zdrój, Poland, September 20–24, 2015

The Microstructure and Thermal Stability of the Two-Component Melt-Spun $Ni_{55}Fe_{20}Cu_5P_{10}B_{10}$ TCMS Amorphous/Amorphous Composite

K. Ziewiec[a,*], M. Wojciechowska[a], K. Prusik[b], D. Mucha[c] and I. Jankowska-Sumara[d]

[a]Institute of Technology, Faculty of Mathematics, Physics and Technical Science, Pedagogical University of Cracow, Podchorążych 2, PL–30084 Kraków, Poland

[b]Faculty of Computer Science and Materials Science, University of Silesia, 75 Pułku Piechoty 1A, PL–41500 Chorzów, Poland

[c]Institute of Catalysis and Surface Chemistry, Polish Academy of Sciences, Niezapominajek 8, PL–30239 Kraków, Poland

[d]Institute of Physics, Pedagogical University, Podchorążych 2, PL–30084 Kraków, Poland

The aim of this study is to present the special features and properties of the two alloys of similar average chemical composition $Ni_{55}Fe_{20}Cu_5P_{10}B_{10}$, processed through two different routes. The first alloy was melt-spun after the ejection of homogeneous liquid using a traditional single chamber crucible, and the second alloy was ejected from a double chamber crucible as two separate liquids: i.e., $Ni_{40}Fe_{40}B_{20}$ and $Ni_{70}Cu_{10}P_{20}$, mixing only at the orifice area. The studies of the microstructure of the composite alloy were performed through the use of transmission electron microscopy and scanning electron microscopy. The $Ni_{55}Fe_{20}Cu_5P_{10}B_{10}$ two-chamber melt-spun (TCMS) alloy, as well as the homogeneous $Ni_{55}Fe_{20}Cu_5P_{10}B_{10}$, $Ni_{40}Fe_{40}B_{20}$, and $Ni_{70}Cu_{10}P_{20}$ alloys, were heated to elevated temperatures and their characteristics studied by means of differential scanning calorimetry. The temperature resistivity change method was applied to the examination of the $Ni_{55}Fe_{20}Cu_5P_{10}B_{10}$ TCMS alloy. The phase composition after heat treatment was investigated using X-ray diffraction. The results of the microstructure examination show that the TCMS alloy is an amorphous/amorphous composite, and is notable for its Ni–Fe–B and Ni–Cu–P stripes resulting from its differentiated chemical composition. Another unique feature of the TCMS alloy is that it retains its wood-like morphology even after high-temperature heat treatment. The crystallisation of the TCMS alloy starts from the Ni–Cu–P constituent and ends with the Ni–Fe–B areas of the sample. The results are discussed on the basis of previous work completed on amorphous matrix composites.

DOI: 10.12693/APhysPolA.130.927

PACS/topics: 61.05.cp, 61.05.J–, 81.05.Kf, 81.05.Pj, 72.15.Cz, 68.60.Dv

1. Introduction

Over the past 50 years, researchers have elaborated upon the many grades of metallic glasses and their many interesting and useful physical, mechanical, and functional properties [1]. However, due to their lack of ductility, as well as to the strenuous requirements regarding the manufacturing equipment and high purity of precursor materials involved in their production, the use of amorphous alloys is still very limited. These limitations can be removed by using low-cost methods for the manufacturing of amorphous/crystalline and amorphous/amorphous composites. The techniques based on low-cost precursors, which enable the controlling of morphology and phase composition, can provide a means for improving the ductility of the metallic glasses [2]. Amorphous/crystalline metallic alloys are based on liquid immiscible alloys [1, 3–6]. An interesting group of two-phase metallic glasses is prepared on the basis of liquid immiscible alloys in such systems as La–Zr–Al–Cu–Ni [7], Nd–Zr–Al–Co [8], and Ni–Nb–Y [7]. The recently-proposed new variation of melt-spinning from a double-chamber crucible [9, 10] causes the formation of a controlled lamellar heterogeneous amorphous/amorphous microstructure. In contrast to amorphous liquid immiscible alloys, in this case the formation of a two-phase glass microstructure does not require a special chemical composition. Furthermore, the amorphous/amorphous alloys should provide interesting microstructure and thermal characteristics. The aim of this work was to reveal the novel properties of the new TCMS alloy produced from $Ni_{40}Fe_{40}B_{20}$ and $Ni_{70}Cu_{10}P_{20}$ melts.

2. Experimental

The samples were prepared based on the following compositions: $Ni_{40}Fe_{40}B_{20}$, $Ni_{70}Cu_{10}P_{20}$, and $Ni_{55}Fe_{20}Cu_5P_{10}B_{10}$. The ingots were prepared starting from 99.95 wt% Ni, 99.95 wt% Fe, and 99.95 wt% Cu, and Ni–P, Cu–P, Ni–B, and Fe–B master alloys. The arc melting was carried out under an argon-gettered protective atmosphere. The alloys were then subjected to melt-spinning in a helium atmosphere, with the linear velocity of the copper roller being 40 m/s and the ejection pressure 150 kPa. The crucible hole diameter was 1.2 mm. The four alloys were produced on the

*corresponding author; e-mail: kziewiec@up.krakow.pl

copper roller. The first was obtained by TCMS using the partition barrier in the crucible [9, 10]. The $Ni_{40}Fe_{40}B_{20}$ and $Ni_{70}Cu_{10}P_{20}$ were processed in the same way [11]. The transmission electron microscopy (TEM) microstructure of the $Ni_{55}Fe_{20}Cu_5P_{10}B_{10}$ TCMS was investigated by means of a JEOL 300kV TEM. The three remaining ribbons, i.e., $Ni_{40}Fe_{40}B_{20}$, $Ni_{70}Cu_{10}P_{20}$, and $Ni_{55}Fe_{20}Cu_5P_{10}B_{10}$ alloys, were ejected from a traditional single-chamber crucible. The samples of the $Ni_{55}Fe_{20}Cu_5P_{10}B_{10}$ TCMS alloy were encapsulated in quartz tubes under vacuum and heated with a constant rate of 5 K/min. The samples were heated to different temperatures: 450, 500, 530, 550, 680, 750, and 800 K. After reaching a given temperature the samples were cooled in water. The cross-section microstructure of the samples was then observed by means of a scanning electron microscope with EDS JEOL 6610, and phase composition was analysed via a X-ray diffractometer using a Siemens D5005 (Bruker-AXS) diffractometer equipped with a Cu radiation. Differential scanning calorimetry (NETZSCH DSC200 F3 MAIA) in an argon and the relative resistivity measurements were used for characterising thermal stability.

3. Results and discussion

The TEM microstructure of the $Ni_{55}Fe_{20}Cu_5P_{10}B_{10}$ TCMS ribbon is shown in Fig. 1, where different contrasting areas may be observed: darker areas are marked A and brighter areas B (Fig. 1a). The electron diffraction patterns (Fig. 1b,c) from both areas show broad diffusive rings typical of amorphous alloys. Both strong diffusive rings have the maximum intensity for a similar radius and correspond to a range of d values between 1.9 Å and 2.3 Å. Different species have a different atomic number; therefore, it is expected that the darker A areas contain more Ni ($Z = 28$) and Cu ($Z = 29$) and the brighter B areas are enriched in Ni ($Z = 28$) and Fe ($Z = 26$). The smooth transitions between area A and area B, without any crystalline phases occurring between them, may suggest that the intermediate compositions between A and B are also amorphous.

SEM images observed on the cross-section of the $Ni_{55}Fe_{20}Cu_5P_{10}B_{10}$ TCMS ribbon in its melt-spun state and after heating to different temperatures, i.e., 450, 500, 530, 550, 680, 750, and 800 K, are shown in Fig. 2. Generally, the microstructures for variants observed directly after melt-spinning (RT) and for temperatures up to 550 K (Fig. 2a) present bright and dark bands arranged along the melt-spinning direction, corresponding to areas of differentiated chemical composition. For higher temperatures of heating, i.e., 680, 750, and 800 K, the contrast between bright and dark bands is smaller, which may be associated with the diffusion of some species, such as boron, at higher temperatures. However, in spite of the weak contrast between bands, the EDS mapping shows that there is no apparent difference in the distribution of Fe, Ni, Cu, and P for RT and for 800 K (Fig. 2b and c). Therefore, in terms of Fe, Ni, Cu, and P concentrations, the alloy has a very stable band-like or wood-like microstructure. Boron was not detected in the analysis, although it is expected that the regions also contain B. During the TCMS process, the streams of Ni–Fe–B and Ni–Cu–P melts were partially mixed while passing through the orifice of the crucible. During rapid cooling, there is no time for extensive diffusion

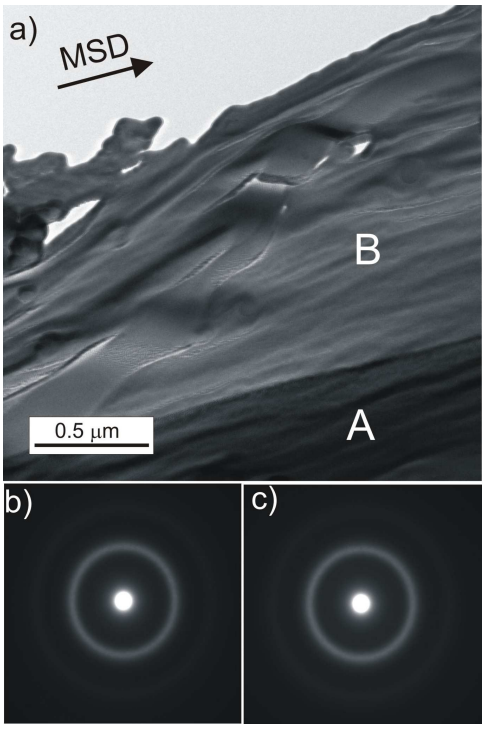

Fig. 1. TEM micrograph for the TCMS $Ni_{55}Fe_{20}Cu_5P_{10}B_{10}$ ribbon: (a) TEM image with the darker areas marked as A and the brighter areas marked as B, (b) electron diffraction pattern from area A, (c) electron diffraction pattern from area B.

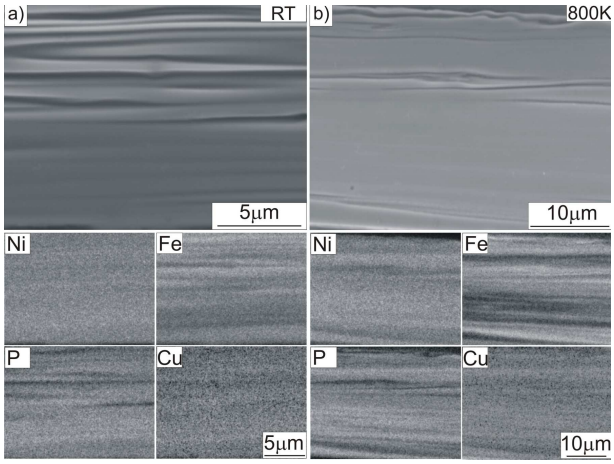

Fig. 2. Microstructure on cross-section of the $Ni_{55}Fe_{20}Cu_5P_{10}B_{10}$ TCMS ribbon prepared for samples after different states of processing: (a) SEM image and EDS mapping for the sample at RT, (b) SEM image and EDS mapping for the sample heated to 800 K.

between the two liquids and the complete homogenisation of the alloy is very unlikely to occur. Furthermore, this chemically-differentiated microstructure is retained even up to 800 K, and homogenisation of the alloy does not occur in spite of crystallisation.

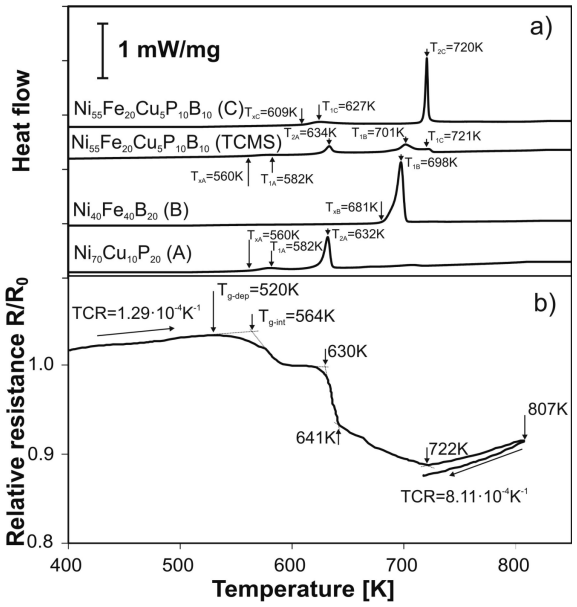

Fig. 3. (a) DSC curves of the amorphous $Ni_{70}Cu_{10}P_{20}$ (A), $Ni_{40}Fe_{40}P_{20}$ (B), $Ni_{55}Fe_{20}Cu_5P_{10}B_{10}$ TCMS, and $Ni_{55}Fe_{20}Cu_5P_{10}B_{10}$ (C) alloys; the symbols T_{xA}, T_{xB}, and T_{xC} denote the onset of crystallisation; the symbols T_{1A}, T_{2A}, T_{3A}, T_{1B}, T_{1C}, and T_{2C} refer to the values of the first, second, and third peaks of the crystallisation sequence observed in the alloys marked A, B (for the homogeneous alloys and the TCMS alloy), and C, respectively, (b) relative resistivity change in the melt-spun $Ni_{55}Fe_{20}Cu_5P_{10}B_{10}$ TCMS ribbon heated at a rate of 5 K/min and during free cooling.

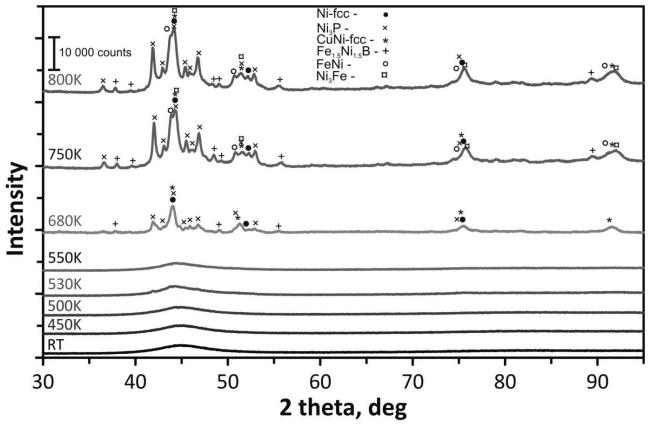

Fig. 4. XRD patterns registered for samples after different states of processing of the $Ni_{55}Fe_{20}Cu_5P_{10}B_{10}$ TCMS alloy: RT — room temperature, denotes melt-spun sample without heat treatment; the samples heated to 450, 500, 530, 550, 680, 750, and 800 K at 5 K/min.

DSC traces of the $Ni_{55}Fe_{20}Cu_5P_{10}B_{10}$ TCMS ribbon and simple melt-spun $Ni_{40}Fe_{40}B_{20}$, $Ni_{70}Cu_{10}P_{20}$, and $Ni_{55}Fe_{20}Cu_5P_{20}$ ribbons are presented in Fig. 3a, which shows the onset of crystallisation and peak temperatures. The largest onset temperature is observed in the $Ni_{40}Fe_{40}B_{20}$ (B) alloy, where $T_{xB} = 681$ K; it also has only one crystallisation peak at $T_{1B} = 698$ K. However, the $Ni_{70}Cu_{10}P_{20}$ (A) alloy presents significantly lower thermal stability, with onset at $T_{xA} = 560$ K. It should be noted that the $Ni_{55}Fe_{20}Cu_5P_{10}B_{10}$ TCMS alloy begins crystallisation at $T_{xA} = 560$ K. This is the same value as the one found for the $Ni_{70}Cu_{10}P_{20}$ alloy. However, the $Ni_{55}Fe_{20}Cu_5P_{10}B_{10}$ ejected from the single-chamber crucible, in spite of its similar average composition, begins crystallisation at a substantially higher temperature, i.e., $T_{xC} = 609$ K. An interesting feature of the $Ni_{55}Fe_{20}Cu_5P_{10}B_{10}$ TCMS alloy is the co-incidental correspondence between peak temperatures found on the DSC trace of this alloy and the traces of the $Ni_{70}Cu_{10}P_{20}$ (A) and $Ni_{40}Fe_{40}B_{20}$ (B) alloys (Fig. 3a). The first crystallisation peak of the $Ni_{55}Fe_{20}Cu_5P_{10}B_{10}$ TCMS alloy is at $T_{1A} = 582$ K, and its maximum is at the same temperature as the first peak for $Ni_{70}Cu_{10}P_{20}$ (A): $T_{1A} = 582$ K. The second peak for the TCMS alloy, $T_{2A} = 634$ K, corresponds to the second peak found in alloy A, i.e., $T_{2A} = 632$ K. The third peak for the TCMS alloy found on the DSC trace at $T_{1B} = 701$ K may be associated with the first and only crystallisation peak for the DSC trace of the B alloy, i.e., $T_{1B} = 698$ K. The fourth DSC peak of the TCMS alloy, occurring at $T_{3A} = 721$ K, is close to the position of the third peak for the C alloy: $T_{2A} = 720$ K. Generally, the DSC study confirms a unique feature of the TCMS $Ni_{55}Fe_{20}Cu_5P_{10}B_{10}$ alloy: that the temperatures of the thermal effects in the alloy are close those of the three amorphous alloys, i.e., A, B, and C. Therefore, TCMS processing enabled the inheriting of the transformations of these alloys. This was not observed in the traditionally melt-spun $Ni_{55}Fe_{20}Cu_5P_{10}B_{10}$ (C) alloy with a homogeneous chemical composition. The presence of the peak at $T_{2C} = 743$ K on the DSC trace of the $Ni_{55}Fe_{20}Cu_5P_{10}B_{10}$ TCMS alloy confirms the presence of the transition regions between the bands of alloy A and alloy B, which are close to the composition of $Ni_{55}Fe_{20}Cu_5P_{10}B_{10}$ (C).

Figure 4b presents changes in the relative electric resistivity (R/R_0) of the $Ni_{55}Fe_{20}Cu_5P_{10}B_{10}$ TCMS alloy recorded at an elevated temperature, matching the same cooling rate as was applied for DSC measurement, i.e., 5 K/min. The starting temperature coefficient of resistivity is measured at a level of 1.29×10^{-4} K^{-1}. The first deviation from linearity (first drop of relative resistivity) occurs at $T_{\mathrm{g-dep}} = 520$ K. This value corresponds to the temperature of glass transformation. The value of $T_{\mathrm{g-int}} = 564$ K observed during resistivity measurements corresponds to the onset of crystallisation, and this value is actually close to the onset of crystallisation for the TCMS alloy and for the alloy A derived from DSC measurement, i.e., $T_{xA} = 560$ K.

The second drop in relative resistivity occurs between 630 K and 641 K, which is co-incidental with the peaks at T_{2A} = 632 K for the A alloy and T_{2A} =632 K for the TCMS alloy. After this stage, above 641 K, resistance decreases at a slower rate, which corresponds to peaks at T_{1B} = 701 K and T_{2C} = 721 K on the DSC curve. After reaching 722 K resistance does not decrease, which suggests that the crystallisation is terminated. The TCR value after heating to 807 K reaches the level of 8.11×10^{-4} K^{-1} during cooling, which is the stable value of TCR. This suggests that the final crystallisation stage has been reached.

The XRD patterns registered for melt-spun and heated ribbons are presented in Fig. 4. The initially amorphous sample remains glassy even at 550 K, where diffraction still has a broad peak between 40° and 50°. The first diffraction peaks confirming the appearance of the crystalline phases are recorded in the sample after heating to 680 K. At this temperature, the peaks can mainly be attributed to three phases. The first phase is isomorphic, with a Ni fcc solid solution (space group Fm-$3m$, a = 3.5238 Å, PDF no. 00-004-0850); the second corresponds to the tetragonal Ni_3P phosphide (space group $I4$, a: 8.956 Å, c: 4.388 Å, PDF no. 04-005-5615); the third may be attributed to a CuNi solid solution (space group Fm-$3m$, a: 3.5636(5) Å, PDF no. 01-071-7832). There are also traces of $Ni_{1.5}Fe_{1.5}B$. Similar phases are also present for the ribbon heated to 750 K and 800 K. However, for these temperatures, a new series of diffraction peaks are present, which may be identified as patterns of the following two phases, i.e., the isomorphic phase with a FeNi fcc solid solution (space group Fm-$3m$, a: 3.575 Å, 01-071-8322), and the fcc $FeNi_3$ phase (space group Fm-$3m$, a: 3.5556 Å, PDF 01-071-8324). The peaks of the orthorhombic $Fe_{1.5}Ni_{1.5}B$ compound (a: 5.34 Å, b: 6.637 Å, c: 4.437 Å, PDF 04-001-9092) are further developed. On this basis, it is found that the crystallisation of the amorphous $Ni_{55}Fe_{20}Cu_5P_{10}B_{10}$ TCMS alloy starts mainly with the formation of the phases containing Ni, Cu, and P; further, the crystallisation of the phases containing Fe and B occurs at higher temperatures.

4. Conclusions

1. TEM, SEM, and XRD observations of the $Ni_{55}Fe_{20}Cu_5P_{10}B_{10}$ TCMS ribbon confirm that the alloy is amorphous and that its wood-like microstructure consists of bands of differentiated chemical composition. The composition of the bands corresponds to the Ni–Cu–P and Ni–Fe–B precursor alloys ejected from the crucible.

2. Despite of the crystallisation of the $Ni_{55}Fe_{20}Cu_5P_{10}B_{10}$ TCMS alloy, the wood-like microstructure of the chemically differentiated microstructure is retained even up to 800 K and homogenisation.

3. DSC and resistivity measurements proved that due to the application of TCMS processing, the alloy of the nominal $Ni_{55}Fe_{20}Cu_5P_{10}B_{10}$ composition inherited the transformations from the $Ni_{70}Cu_{10}P_{20}$ and $Ni_{40}Fe_{40}B_{20}$ precursor alloys in their amorphous state, which was not observed in the traditionally melt-spun homogeneous $Ni_{55}Fe_{20}Cu_5P_{10}B_{10}$ alloy.

4. There is no apparent crystallisation in the $Ni_{55}Fe_{20}Cu_5P_{10}B_{10}$ TCMS alloy heated to temperatures up to 550 K. Heating at 680 K caused the formation of mainly a Ni fcc solid solution, tetragonal Ni_3P phosphide, and CuNi solid solution, which corresponds to crystallisation of the Ni–Cu–P constituent of the composite alloy. Heating to higher temperatures resulted in the formation of a FeNi fcc solid solution, fcc $FeNi_3$ phase, and orthorhombic $Fe_{1.5}Ni_{1.5}B$ compound as a result of crystallization of the Ni–Fe–B constituent of the alloy.

Acknowledgments

The study was supported by National Science Centre (NCN) under project No. 2012/05/B/ST8/02644.

References

[1] H. Warlimont, *Mater. Sci. Eng. A* **304–306**, 61 (2001).

[2] W.H. Wang, *J. Non-Cryst. Solids* **351**, 1481 (2005).

[3] M.F. Ashby, A.L. Greer, *Scr. Mater.* **54**, 321 (2006).

[4] R. Schäfer, *J. Magn. Magn. Mater.* **215–216**, 652 (2000).

[5] P.K. Liaw, G. Wang, J. Schneider, *JOM* **62**, 69 (2010).

[6] A.A. Kündig, M. Ohnuma, D.H. Ping, T. Ohkubo, K. Hono, *Acta Mater.* **52**, 2441 (2004).

[7] E.S. Park, E.Y. Jeong, J.K. Lee, J.C. Bae, A.R. Kwon, A. Gebert, L. Schultz, H.J. Chang, D.H. Kim, *Scr. Mater.* **56**, 197 (2007).

[8] A. Concustell, N. Mattern, H. Wendrock, U. Kuehn, A. Gebert, J. Eckert, A.L. Greer, J. Sort, M.D. Baro, *Scr. Mater.* **56**, 85 (2007).

[9] K. Ziewiec, K. Prusik, K. Bryła, A. Ziewiec, *Solid State Phenom.* **203–204**, 361 (2013).

[10] K. Ziewiec, Z. Kędzierski, A. Zielińska-Lipiec, J. Stępiński, S. Kąc, *J. Alloys Comp.* **615**, S29 (2014).

[11] K. Ziewiec, M. Wojciechowska, A. Błachowski, K. Ruebenbauer, I. Jankowska-Sumara, K. Prusik, D. Mucha, J. Latuch, *Intermetallics* **65**, 15 (2015).